Journal of Solid State Chemistry **155,** 243–249 (2000)
doi:10.1006/jssc.2000.8960, available online at http://www.idealibrary.com on IDEAL®

Structures and Conductivities of the Quaternary *A*/Bi/Cu/S Phases KBi_2CuS_4 and $A_3Bi_5Cu_2S_{10}$ (*A*=Rb, Cs)[1]

Yuting Yang,* Paul Brazis,† Carl R. Kannewurf,† and James A. Ibers*

*Department of Chemistry and †Department of Electrical & Computer Engineering, Northwestern University, 2145 Sheridan Rd., Evanston, Illinois 60208-3113

Received May 24, 2000; in revised form August 29, 2000; accepted September 5, 2000

DEDICATED TO PROFESSOR J. M. HONIG

The compounds KBi_2CuS_4, $Cs_3Bi_5Cu_2S_{10}$, and $Rb_3Bi_5Cu_2S_{10}$ were prepared by stoichiometric reactions of the corresponding alkali-metal sulfides with Bi, Cu, and S at 1123 K. KBi_2CuS_4 crystallizes as a racemic twin in space group $Cmc2_1$ of the orthorhombic system with four formula units in a cell of dimensions $a = 4.0273(8)$, $b = 13.770(3)$, $c = 14.259(3)$ Å at 153 K; $A_3Bi_5Cu_2S_{10}$ (A = Cs or Rb) are isostructural and crystallize in a new structure type in space group $Pnnm$ with two formula units in cells of dimensions $a = 14.571(3)$, $b = 17.819(4)$, $c = 4.0686(8)$ Å for $Rb_3Bi_5Cu_2S_{10}$ and $a = 15.041(3)$, $b = 17.994(3)$, $c = 4.0973(8)$ Å for $Cs_3Bi_5Cu_2S_{10}$ at 153 K. These are channel structures with the alkali-metal cations located in channels formed by edge sharing of distorted Bi octahedra and distorted Cu tetrahedra. Electrical conductivity measurements on KBi_2CuS_4 and $Rb_3Bi_5Cu_2S_{10}$ indicate that both materials are semiconducting. The conductivity of KBi_2CuS_4 is two orders of magnitude higher than that of $Rb_3Bi_5Cu_2S_{10}$ at room temperature. KBi_2CuS_4 undergoes a transition from an *n*- to a *p*-type semiconductor at 210 K as determined by thermopower measurements. © 2000 Academic Press

INTRODUCTION

Many bismuth-containing ternary and quaternary chalcogenides are known. Some occur in nature, for example, Pb/Bi/Cu/S phases (1–5), which are most often structural derivatives of bismuthinite Bi_2S_3 and aikinite $PbBiCuS_3$. These exhibit Pb/Bi disorder and partial occupancy of interstices by Cu (6–8). The ternary phases A/Bi/Q (A = alkali or alkaline-earth metal; Q = S, Se, or Te) include, to name a few, two phases of $CsBiS_2$ (9), $RbBi_3S_5$ (10), $ABiS_2$ (11) (A = Na, K), $K_2Bi_8S_{13}$ (12), $K_2Bi_8Se_{13}$(13), $Ba_3Bi_{6.67}Se_{13}$ (14), and $CsBi_4Te_6$ (15). Ternary phases Bi/Cu/Q include $CuBi_5S_8$ (16), Cu_3BiS_3 (17), and $CuBiS_2$ (18). Bi atoms are coordinated by six or seven Q atoms. Usually they have five close Q neighbors in a square pyramid with Bi near the center of the basal plane with the sixth Q atom further away to complete a distorted octahedron or the sixth and seventh Q atoms further away to complete a capped octahedron with one vertex split in two (8).

The ionic radius of the Bi^{3+} cation is 1.03 Å, the same as La^{3+} (1.032 Å) (19) and larger than the other rare earths (*Ln*). Both Bi^{3+} and La^{3+} can be octahedrally coordinated by chalcogens, but Bi^{3+} has a stereoactive lone pair of electrons. Nevertheless, some $ALn_{1\pm x}Bi_{4\pm x}S_8$ phases have been discovered that show disorder between *Ln* and Bi (20). But it remains of interest to compare Bi compounds with related rare-earth (*Ln*) compounds. A number of A/*Ln*/Cu/Q (Q = S, Se, or Te) phases are known, including $K_2Cu_2CeS_4$ (21), $KCuCe_2S_6$ (21), $CsCuCeS_3$ (22), $K_2AgCeTe_4$ (23), $KCuGd_2S_4$ (24), and $Rb_2Cu_3CeTe_5$ (25). Here we investigate the corresponding A/Bi/Cu/S system and report the phases KBi_2CuS_4 and $A_3Bi_5Cu_2S_{10}$ (A = Rb, Cs).

EXPERIMENTAL

Syntheses

A_2S_n ($n = 1$ or 3) were prepared by the reaction of K (99.95%, Alfa Aesar), Rb (99.8%, Alfa Aesar), or Cs (99.8%, Alfa Aesar) with S (99.5%, Alfa Aesar) in liquid ammonia. The compounds KBi_2CuS_4, $Rb_3Bi_5Cu_2S_{10}$, and $Cs_3Bi_5Cu_2S_{10}$ were prepared by the reactions of stoichiometric amounts of A_2S_n, Bi (99.999%, Alfa Aesar), Cu (99.5%, Alfa Aesar), and S in fused-silica tubes. These tubes were maintained at 1123 K for 7 days, and then slowly cooled to room temperature at a rate of 3 K/h. Air-stable black flat needles for KBi_2CuS_4 and black needles of $A_3Bi_5Cu_2S_{10}$ (A = Rb, Cs) were obtained in yields of about 50%. No attempt was made to optimize these yields. Other phases present were Bi_2S_3 and some ternaries. EDX analysis with a Hitachi S4500 scanning electron microscope confirmed the presence of all four elements with approximate ratio 1/2/1/4 for KBi_2CuS_4 and 3/5/2/10 for $A_3Bi_5Cu_2S_{10}$, respectively.

[1]Dedicated to George Honig, as friendly and helpful an editor as they come.

0022-4596/00 $35.00

Crystallography

Diffraction data from single crystals were collected at 153 K on a Bruker Smart-1000 CCD diffractometer (26) at 20 s for each frame and 0.25° in ω. Face-indexed absorption corrections were applied to all data sets (26). The data were further corrected for frame variations with the use of the program SADABS (26).

Systematic absences and Laue symmetry led to the orthorhombic space groups $Cmc2_1$ or $Cmcm$ for KBi_2CuS_4. Intensity statistics strongly favor the noncentrosymmetric space group. Indeed, with the use of the program SHELXS (27) no solution could be found in space group $Cmcm$ by direct methods or by means of a sharpened Patterson function, but a solution was readily found in space group $Cmc2_1$. The structure was refined by full-matrix least-squares methods with the program SHELXL in the SHELXTL-97 suite (27). The Flack parameter was near 0.5, suggesting either a racemic twin or the possibility that the true space group is $Cmcm$. However, examination of the resultant atomic coordinates with the program MISSYM (28) indicated that the positions of both Bi and S(1) atoms are inconsistent with an inversion center. The resultant KBi_2CuS_4 structure ($Cmc2_1$) is a slight distortion of the KGd_2CuS_4 ($Cmcm$) structure (24). The refined cell parameters and other relevant crystal data for KBi_2CuS_4 are given in Table 1, and the final atomic parameters and equivalent isotropic displacement parameters are given in Table 2.

Systematic absences and Laue symmetry led to the orthorhombic space group $Pnnm$ or $Pnn2$ for the compounds $Rb_3Bi_5Cu_2S_{10}$ and $Cs_3Bi_5Cu_2S_{10}$. The structures were solved and refined successfully in the centrosymmetric space group $Pnnm$. Relevant crystal data are given in Table 1 and final atomic parameters and equivalent isotropic displacement parameters are given in Table 3.

TABLE 1
Crystal Data ($T = 153$ K) and Structure Refinements for KBi_2CuS_4, $Cs_3Bi_5Cu_2S_{10}$, and $Rb_3Bi_5Cu_2S_{10}$

Formula	KBi_2CuS_4	$Rb_3Bi_5Cu_2S_{10}$	$Cs_3Bi_5Cu_2S_{10}$
Formula weight	648.84	1748.99	1891.31
Space group	$Cmc2_1$	$Pnnm$	$Pnnm$
a (Å)	4.0273(8)	14.571(3)	15.041(3)
b (Å)	13.770(3)	17.819(4)	17.994(4)
c (Å)	14.259(3)	4.0686(8)	4.0973(8)
Volume (Å^3)	790.8(3)	1056.4(4)	1108.9(4)
Z, ρ_c (g/cm^3)	4, 5.450	2, 5.498	2, 5.664
μ (cm^{-1})	485.39	513.01	471.84
Transmission factors	0.064–0.39	0.14–0.61	0.077–0.38
θ range (°)	2.86–28.23	1.81–28.51	1.76–28.69
Data/parameters	1035/51	1438/64	1547/64
Goodness-of-fit on F^2	0.832	0.899	0.895
R_1 [$I > 2\sigma(I)$][a]	0.0173	0.0233	0.0247
wR_2 (all data)[b]	0.0427	0.0604	0.0621

[a] $R_1 = \sum \| F_o| - |F_c \| / |F_o|$.
[b] $wR_2 = \{\sum[w(F_o^2 - F_c^2)^2] / \sum wF_o^4\}^{1/2}$; $w^{-1} = \sigma^2(F_o^2) + (0.04 \times F_o^2)^2$ for $F_o^2 \geq 0$ and $w^{-1} = \sigma^2(F_o^2)$ for $F_o^2 < 0$.

TABLE 2
Atomic Coordinates[a] and Equivalent Isotropic Displacement Parameters (Å^2) for KBi_2CuS_4

Atom	y	z	U^b
Bi(1)	0.38567(3)	0.17649(2)	0.0110(1)
Bi(2)	0.65449(2)	0.29311(2)	0.0112(1)
Cu(1)	0.1484(1)	0.4798(1)	0.0147(3)
K(1)	0.1122(2)	0.0045(2)	0.0163(5)
S(1)	0.0168(2)	0.2255(2)	0.0148(5)
S(2)	0.2556(2)	0.6320(2)	0.0113(4)
S(3)	0.2681(2)	0.3630(2)	0.0103(4)
S(4)	0.4318(2)	−0.0001(2)	0.0119(5)

[a] $x = 0$ for all atoms.
[b] U is defined as one-third of the trace of the orthogonalized U_{ij} tensor.

Electrical Conductivity and Thermopower Measurements

The electrical conductivities of single crystals of KBi_2CuS_4 and $Rb_3Bi_5Cu_2S_{10}$ were measured by a four-probe technique (29) . Electrical contacts consisted of fine gold wire (25 and 60 μm diameter) attached to the crystals with gold paste. Samples were placed under vacuum for at least 24 h to allow the gold paste to cure completely, which improved contact performance. Excitation currents were kept as low as possible, typically at or below 1 μA, in order to minimize any nonohmic voltage response and thermoelectric effects at the contact-sample interface.

TABLE 3
Atomic Coordinates[a] and Equivalent Isotropic Displacement Parameters (Å^2) for $Rb_3Bi_5Cu_2S_{10}$ and $Cs_3Bi_5Cu_2S_{10}$

	$Rb_3Bi_5Cu_2S_{10}$			$Cs_3Bi_5Cu_2S_{10}$		
Atom	x	y	U	x	y	U
Bi(1)	0.28395(2)	0.59504(2)	0.0106(1)	0.28831(3)	0.59151(2)	0.0157(1)
Bi(2)	0.73665(3)	0.10284(2)	0.0124(1)	0.74363(3)	0.10470(2)	0.0189(1)
Bi(3)	0.00	0.00	0.0172(2)	0.00	0.00	0.0252(2)
A(1)	0.47639(6)	0.25078(5)	0.0154(2)	0.47766(5)	0.24745(4)	0.0223(2)
A(2)	0.00	0.5000	0.0137(3)	0.00	0.5000	0.0243(2)
Cu(1)	0.21828(8)	0.24323(7)	0.0163(3)	0.2195(1)	0.23975(8)	0.0259(3)
S(1)	0.0954(2)	0.1380(1)	0.0106(5)	0.0970(2)	0.1348(1)	0.0159(5)
S(2)	0.1268(2)	0.3512(1)	0.0122(5)	0.1379(2)	0.3501(1)	0.0179(5)
S(3)	0.2018(2)	0.7255(1)	0.0122(5)	0.2063(2)	0.7193(1)	0.0170(5)
S(4)	0.3312(2)	0.0332(1)	0.0111(5)	0.3224(2)	0.0288(1)	0.0168(5)
S(5)	0.3814(2)	0.4409(1)	0.0150(5)	0.3855(2)	0.4397(2)	0.0235(6)

[a] $z = 0$ for all atoms.

Variable-temperature thermopower data for KBi_2CuS_4 were collected with the slow-ac measurement technique (30). The measurement apparatus featured Au (0.07% Fe)/Chromel differential thermocouples for monitoring the applied temperature gradients. Fine gold wire (10 μm in diameter) was used for sample voltage contacts, which were made as long as possible in order to minimize thermal conduction through the leads. The sample and thermocouple voltages were measured with Keithley Model 2182 and Keithley Model 182 nanovoltmeters, respectively. The applied temperature gradient was in the range from 0.1 to 0.4 K. Measurements were taken under a turbopumped vacuum maintained below 10^{-5} Torr. The sample chamber was evacuated for 1–3 h prior to cooling to remove any residual water vapor or solvents from the gold paste. Owing to increased Johnson noise from highly resistive samples, these thermopower measurements are limited to samples with a resistance below approximately 1 MΩ; $Rb_3Bi_5Cu_2S_{10}$ is too resistive, and thermopower measurements were limited to KBi_2CuS_4 samples above 80 K.

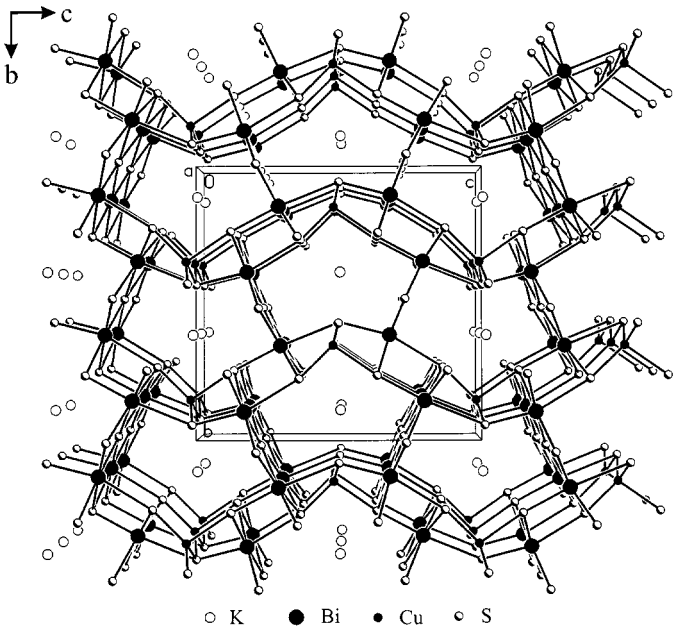

FIG. 1. Structure of KBi_2CuS_4.

RESULTS AND DISCUSSION

The structure of KBi_2CuS_4 is shown in Fig. 1 and a polyhedral view is given in Fig. 2. KBi_2CuS_4 has a channel structure with the K^+ cations in the channel in a capped trigonal prism of S atoms. Two crystallographically distinct Bi atoms are located in distorted octahedra. Selected bond lengths and angles for KBi_2CuS_4 are given in Table 4. The Bi(1)–S bond lengths range from 2.597(3) to 3.114(3) Å, with three short bonds (2.597(3), 2.794(2) × 2 Å) on one side and three comparatively longer ones (2.871(2) × 2, 3.114(3) Å) on the other side. The Bi(2)–S bond lengths range from 2.610(3) to 3.179(3) Å, with three short (2.610(3), 2.738(2) × 2 Å) and three longer bonds (2.929(2) × 2, 3.179(3) Å). These are in a reasonable range for Bi–S bond lengths, such as 2.57(2) to 3.34(2) Å in $KBi_{6.33}S_{10}$ and 2.61(1) to 3.38(2) Å in $K_2Bi_8S_{13}$ (12). In the present structure the bond angles in the Bi octahedra range from 80.58(6) to 97.03(7)°. The Cu–S bond lengths are also reasonable, from 2.315(2) to 2.624(3) Å, compared with 2.372(1)–2.398(1) Å in $BaLaCuS_3$ (31). The CuS_4 tetrahedron is also distorted with one Cu–S bond length about 0.3 Å longer than the others.

KBi_2CuS_4 has a structure that is distorted from that of KGd_2CuS_4 (24). In KGd_2CuS_4 the one independent Gd^{3+} site is located in a distorted octahedron of S atoms. Although the bond lengths of Gd^{3+} can also be considered as a group of three short bonds, 2.731(2), 2.741(2) × 2 Å, and three longer bonds, 2.778(2), 2.834(1) × 2 Å, these differences are much less pronounced than they are for the Bi bond lengths in KBi_2CuS_4. The anisotropy of the Bi–S bond lengths arises from the stereochemically active lone pair of electrons on Bi^{3+}, which presumably points toward the long-bond side (32).

The ionic radii of Cs, Rb, K, and Na are 1.67, 1.52, 1.38, and 1.02 Å, respectively (19). Cs and Rb are probably too large to fit into the presumed rigid channels of KBi_2CuS_4, as we were unable to prepare ABi_2CuS_4 (A = Rb, Cs), but instead $A_3Bi_5Cu_2S_{10}$ resulted. Na may be too small; in fact, we were unable to prepare any Na/Bi/Cu/S phase.

$Cs_3Bi_5Cu_2S_{10}$ and $Rb_3Bi_5Cu_2S_{10}$ are isostructural. The structure of $Cs_3Bi_5Cu_2S_{10}$ is shown in Fig. 3 and a polyhedral representation is given in Fig. 4. Selected bond lengths

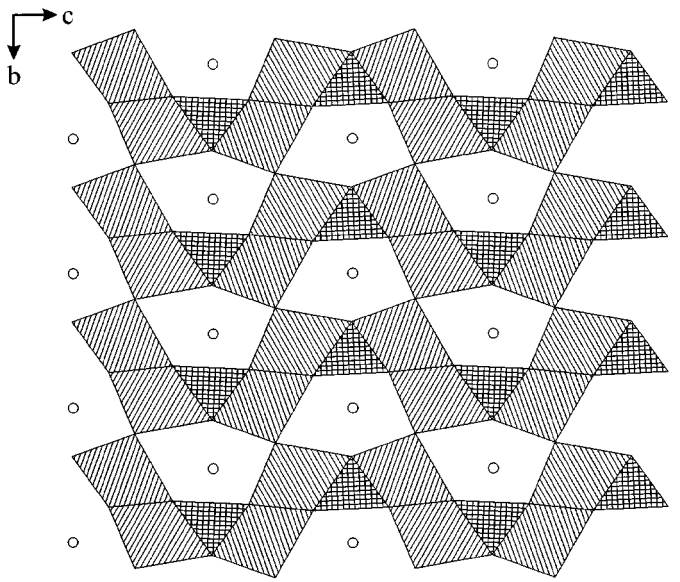

FIG. 2. Polyhedral view of KBi_2CuS_4.

TABLE 4
Bond Lengths and Angles for KBi_2CuS_4

Bond lengths (Å)				Bond angles (°)			
Bi(1)–S(4)	2.597(3)	Cu(1)–S(4)×2	2.315(2)	S(4)–Bi(1)–S(1)×2	94.84(7)	S(2)–Bi(2)–S(1)×2	90.99(7)
Bi(1)–S(1)×2	2.794(2)	Cu(1)–S(3)	2.343(3)	S(1)–Bi(1)–S(1)	92.24(8)	S(3)–Bi(2)–S(1)×2	174.47(7)
Bi(1)–S(2)×2	2.871(2)	Cu(1)–S(2)	2.624(3)	S(4)–Bi(1)–S(2)×2	87.22(7)	S(3)–Bi(2)–S(1)×2	89.08(5)
Bi(1)–S(3)	3.114(3)	K(1)–S(4)×2	3.198(3)	S(1)–Bi(1)–S(2)×2	177.31(8)	S(1)–Bi(2)–S(1)	86.88(7)
Bi(2)–S(2)	2.610(3)	K(1)–S(2)×2	3.268(3)	S(1)–Bi(1)–S(2)×2	89.30(5)	S(4)–Bi(2)–S(2)	173.63(8)
Bi(2)–S(3)×2	2.738(2)	K(1)–S(3)×2	3.293(3)	S(2)–Bi(1)–S(2)	89.08(8)	S(4)–Bi(2)–S(3)×2	82.87(6)
Bi(2)–S(1)×2	2.929(2)	K(1)–S(1)	3.414(4)	S(4)–Bi(1)–S(3)	162.83(7)	S(4)–Bi(2)–S(1)×2	93.63(7)
Bi(2)–S(4)	3.179(3)			S(1)–Bi(1)–S(3)×2	97.03(7)	S(4)–Cu(1)–S(4)	120.9(1)
				S(2)–Bi(1)–S(3)×2	80.58(6)	S(4)–Cu(1)–S(3)×2	115.06(7)
				S(2)–Bi(2)–S(3)×2	92.84(7)	S(4)–Cu(1)–S(2)×2	99.58(8)
				S(3)–Bi(2)–S(3)	94.70(8)	S(3)–Cu(1)–S(2)	101.1(1)

and angles of $Cs_3Bi_5Cu_2S_{10}$ and $Rb_3Bi_5Cu_2S_{10}$ are given in Tables 5 and 6, respectively. The Bi–S bond lengths are reasonable, ranging from 2.615(2) to 3.188(3) Å in $Rb_3Bi_5Cu_2S_{10}$, and from 2.599(3) to 3.256(3) Å in $Cs_3Bi_5Cu_2S_{10}$. Cu–S bond lengths are also reasonable, from 2.340(3) to 2.593(3) Å in $Rb_3Bi_5Cu_2S_{10}$ and from 2.334(3) to 2.639(3) Å in $Cs_3Bi_5Cu_2S_{10}$. Similar bond angle distortions were observed for the Bi octahedron ranging from 82.88(6) to 97.06(7)° in $Rb_3Bi_5Cu_2S_{10}$ and from 81.03(6) to 97.81(9)° in $Cs_3Bi_5Cu_2S_{10}$.

The structure of $A_3Bi_5Cu_2S_{10}$ (A = Rb and Cs) is closely related to that of KBi_2CuS_4, which can be thought of as containing edge-sharing BiS_6–BiS_6–CuS_4 chains parallel to c. Such chains are interconnected in the b direction by S atoms to form the channels. The structure of $A_3Bi_5Cu_2S_{10}$ has similar chains but the middle BiS_6 octahedron shares

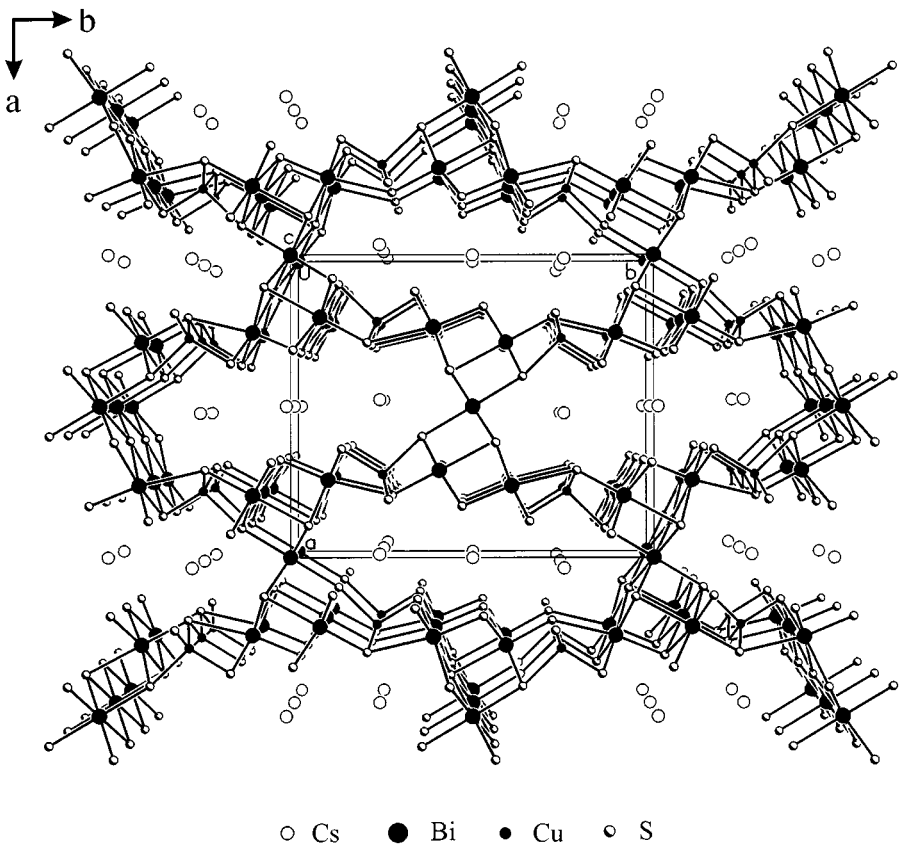

FIG. 3. Structure of $Cs_3Bi_5Cu_2S_{10}$.

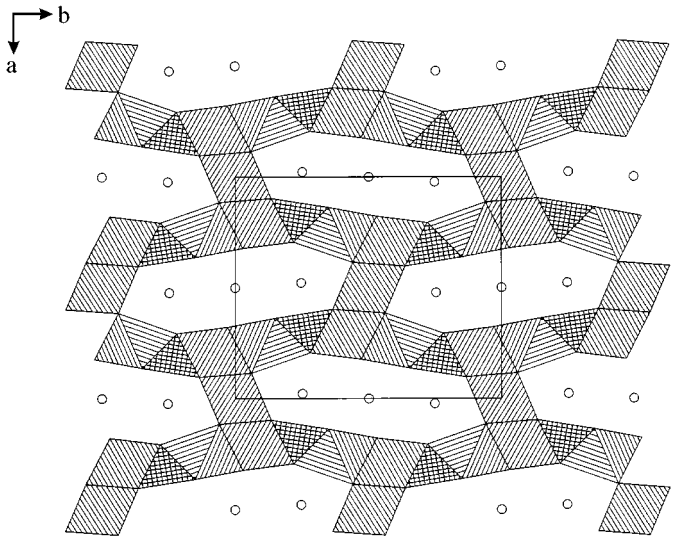

FIG. 4. Polyhedral view of $Cs_3Bi_5Cu_2S_{10}$.

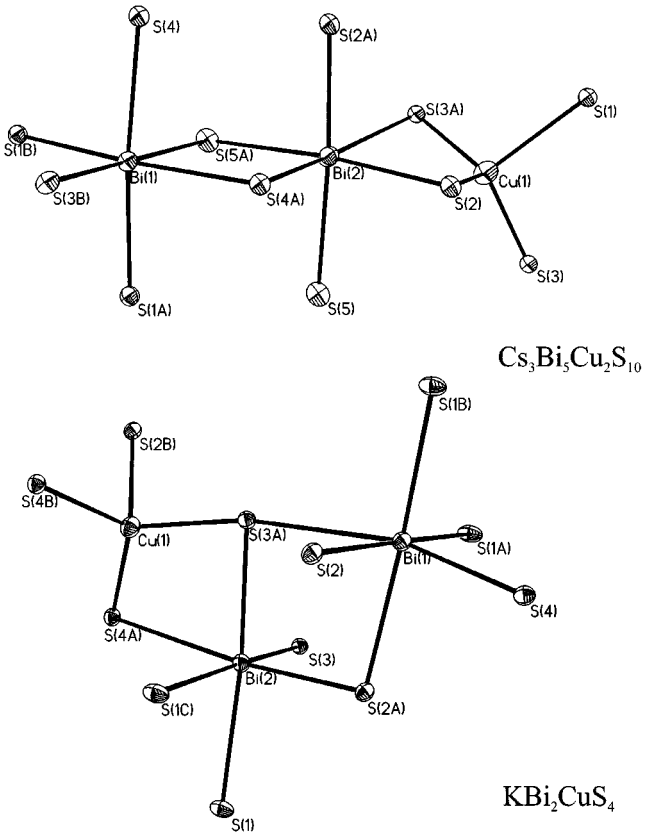

FIG. 5. The BiS_6–BiS_6–CuS_4 unit in $Cs_3Bi_5Cu_2S_{10}$ and KBi_2CuS_4.

opposite edges with the other BiS_6 octahedron and the CuS_4 tetrahedron whereas in KBi_2CuS_4 it shares neighboring edges, as illustrated in Fig. 5. In the *b* direction the resultant channel is larger in $A_3Bi_5Cu_2S_{10}$. These chains are interconnected by additional BiS_6 octahedra so that the channels are also extended in the *a* direction. The channel size is about 7.5×18 Å in $Cs_3Bi_5Cu_2S_{10}$, large enough to accommodate Rb^+ or Cs^+, whereas it is about 6.9×7.1 Å in KBi_2CuS_4. We would expect the corresponding rare-earth phases $A_3Ln_5Cu_2S_{10}$ to be stable, but such phases have not been reported.

In the unit cell of $A_3Bi_5Cu_2S_{10}$ there are two *A*(1) atoms and one *A*(2) atom in each channel. The *A*(1)S_7 polyhedron is a capped trigonal prism whereas the *A*(2)S_6 polyhedron is a trigonal prism, a rare coordination environment for Rb^+ or Cs^+, but one seen, for example, in $Cs_4Ta_2S_{11}$ and $Cs_4Nb_2S_{11}$ (33). Not surprisingly, the bond lengths decrease as the coordination number of *A* decreases from 7 to 6, for example $3.403(3) \times 2$ and $3.406(2)$ Å $\times 4$ for the CsS_6 polyhedron compared with $3.452(2) \times 2$, $3.480(2) \times 2$, $3.617(2) \times 2$, and 3.727(3) Å for the CsS_7 polyhedron.

Both KBi_2CuS_4 and $Rb_3Bi_5Cu_2S_{10}$ are semiconductors. The conductivity of KBi_2CuS_4 drops two orders of magnitude between 298 K and 4.2 K (Fig. 6) and that for $Rb_3Bi_5Cu_2S_{10}$ decreases even more rapidly. Below approximately 200 K the data for KBi_2CuS_4 show a soft minimum near or slightly below 150 K, and a more rapid decrease

TABLE 5
Bond Lengths (Å) for $Rb_3Bi_5Cu_2S_{10}$ and $Cs_3Bi_5Cu_2S_{10}$

	$Rb_3Bi_5Cu_2S_{10}$	$Cs_3Bi_5Cu_2S_{10}$		$Rb_3Bi_5Cu_2S_{10}$	$Cs_3Bi_5Cu_2S_{10}$
Bi(1)–S(3)	2.615(2)	2.609(3)	*A*(1)–S(1)×2	3.328(2)	3.452(2)
Bi(1)–S(1)×2	2.796(2)	2.789(2)	*A*(1)–S(3)×2	3.329(2)	3.480(2)
Bi(1)–S(4)×2	2.858(2)	2.871(2)	*A*(1)–S(2)×2	3.499(2)	3.617(2)
Bi(1)–S(5)	3.092(3)	3.098(3)	*A*(1)–S(5)	3.659(3)	3.727(3)
Bi(2)–S(4)	2.618(2)	2.599(3)	*A*(2)–S(2)×2	3.233(2)	3.403(3)
Bi(2)–S(2)×2	2.715(2)	2.719(2)	*A*(2)–S(4)×4	3.246(2)	3.406(2)
Bi(2)–S(5)×2	3.033(2)	3.064(2)	Cu(1)–S(2)	2.340(3)	2.334(3)
Bi(2)–S(3)	3.188(3)	3.256(3)	Cu(1)–S(3)×2	2.365(1)	2.362(2)
Bi(3)–S(1)×2	2.825(2)	2.830(3)	Cu(1)–S(1)	2.593(3)	2.639(3)
Bi(3)–S(5)×4	2.869(2)	2.888(2)			

TABLE 6
Bond Angles (°) for $Rb_3Bi_5Cu_2S_{10}$ and $Cs_3Bi_5Cu_2S_{10}$

	$Rb_3Bi_5Cu_2S_{10}$	$Cs_3Bi_5Cu_2S_{10}$		$Rb_3Bi_5Cu_2S_{10}$	$Cs_3Bi_5Cu_2S_{10}$
S(3)–Bi(1)–S(1)×2	92.54(6)	92.66(7)	S(3)–Bi(2)–S(4)	174.13(7)	170.92(7)
S(1)–Bi(1)–S(1)	93.38(7)	94.55(8)	S(3)–Bi(2)–S(2)×2	82.88 (6)	81.03(6)
S(3)–Bi(1)–S(4)×2	94.25(6)	94.15(7)	S(3)–Bi(2)–S(5)×2	92.92 (6)	95.31(6)
S(1)–Bi(1)–S(4)×2	173.10(7)	172.99(7)	S(1)–Bi(3)–S(1)	180	180
S(1)–Bi(1)–S(4)×2	87.54(5)	86.80(6)	S(1)–Bi(3)–S(5)×4	91.33(6)	89.18(7)
S(4)–Bi(1)–S(4)	90.75(7)	91.05(7)	S(1)–Bi(3)–S(5)×4	88.67(6)	90.82(7)
S(3)–Bi(1)–S(5)	179.89(7)	179.93(8)	S(5)–Bi(3)–S(5)	180	180
S(1)–Bi(1)–S(5)×2	87.39(6)	87.38(6)	S(5)–Bi(3)–S(5)×2	90.31(7)	90.35(8)
S(4)–Bi(1)–S(5)×2	85.83(5)	85.81(6)	S(5)–Bi(3)–S(5)×2	89.69(7)	89.65(8)
S(4)–Bi(2)–S(2)×2	93.26(6)	93.05(7)	S(5)–Bi(3)–S(5)	180	180
S(2)–Bi(2)–S(2)	97.06(7)	97.81(9)	S(2)–Cu(1)–S(3)×2	112.97(7)	112.41(7)
S(4)–Bi(2)–S(5)×2	91.43(6)	91.43(7)	S(3)–Cu(1)–S(3)	118.7(1)	120.3(1)
S(2)–Bi(2)–S(5)×2	172.00(5)	171.68(6)	S(2)–Cu(1)–S(1)	101.61(9)	104.0(1)
S(2)–Bi(2)–S(5)×2	89.14(5)	88.95(6)	S(3)–Cu(1)–S(1)×2	104.08(7)	102.60(7)
S(5)–Bi(2)–S(5)	84.26(6)	83.93(7)			

below 50 K. For neither compound could the complete conductivity data be fit to either an Arrhenius or a hopping model. Therefore, the band gaps could not be evaluated from conductivity measurements. However, the slope of the conductivity curve of $Rb_3Bi_5Cu_2S_{10}$ is larger than that for KBi_2CuS_4, suggesting that $Rb_3Bi_5Cu_2S_{10}$ may have a higher activation energy.

Above 210 K the thermopower of KBi_2CuS_4 steadily increases with increasing temperature (Fig. 7) and shows *n*-type behavior. Below 210 K, the thermoelectric response is positive, indicating p-type behavior. The electrical conductivity (Fig. 6) shows a change in slope at the point where the thermopower crosses through zero. Below 170 K the slope of the thermopower reverses direction and its magnitude again decreases as the temperature decreases. This change occurs in the same temperature range where the local minimum occurs in the conductivity. A soft change in slope of the thermopower data is also seen between 250 and 270 K, but no correlation with the behavior of the electrical conductivity could be identified. The transition from *n*- to *p*-type at 210 K does not correlate with a phase transition since the structure determined from X-ray data collected at room temperature agrees well with the one at low temperature.

KBi_2CuS_4 exhibits extrinsic semiconducting behavior, as deduced from both the conductivity and thermopower data. At high temperature, the electrons in the conduction band dominate the transport properties, and the material exhibits *n*-type behavior; at low temperature, electrons in the

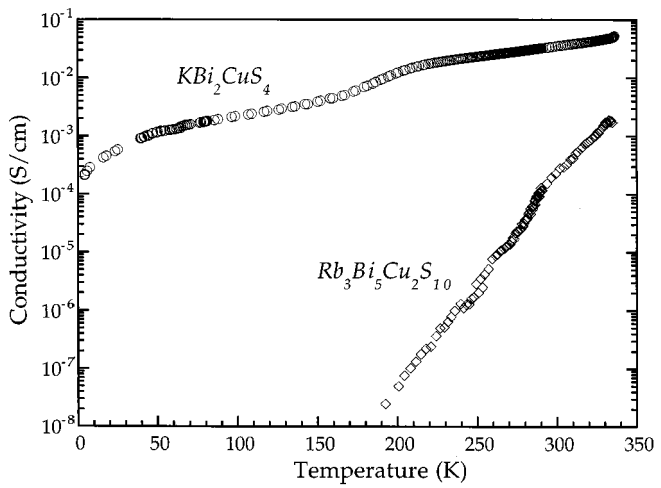

FIG. 6. Temperature dependence of the conductivity for KBi_2CuS_4 and $Rb_3Bi_5Cu_2S_{10}$.

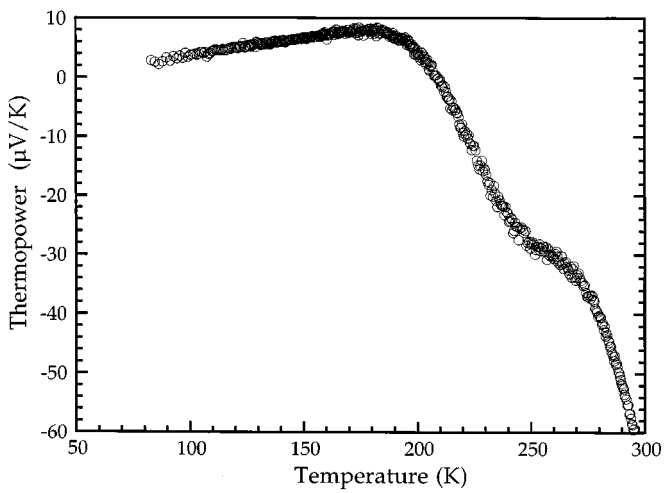

FIG. 7. Temperature dependence of the thermopower for KBi_2CuS_4.

conduction band are few, charge transport is dominated by the positive holes, and *p*-type behavior results, perhaps from small numbers of cation or anion vacancies in the structure. Hall effect measurements are needed for a better understanding of these transport properties, but the high resistivity and small size of the crystals make such measurements difficult.

ACKNOWLEDGMENTS

This work made use of facilities supported by the MRSEC program of the National Science Foundation (DMR96-32472) at the Materials Research Center of Northwestern University. This research was supported by the National Science Foundation through Grant DMR 97-09351. We are grateful to Dr. Olivier Tougait for his helpful discussions.

REFERENCES

1. I. Kohatsu and B. J. Wuensch, *Acta Crystallogr. Sect. B Struct. Crystallogr. Cryst. Chem.* **27,** 1245–1252 (1971).
2. M. Ohmasa and W. Nowacki, *Z. Kristallogr. Kristallgeom. Kristallphys. Kristallchem.* **132,** 71–86 (1970).
3. I. Kohatsu and B. J. Wuensch, *Z. Kristallogr. Kristallgeom. Kristallphys. Kristallchem.* **138,** 343–365 (1973).
4. W. G. Mumme, *Am. Mineral.* **60,** 300–308 (1975).
5. W. G. Mumme, *Am. Mineral.* **60,** 548–558 (1975).
6. H. Horiuchi and B. J. Wuensch, *Can. Mineral.* **14,** 536–539 (1976).
7. H. Horiuchi and B. J. Wuensch, *Can. Mineral.* **15,** 527–535 (1977).
8. I. Kohatsu and B. J. Wuensch, *Acta Crystallogr. Sect. B Struct. Crystallogr. Cryst. Chem.* **32,** 2401–2409 (1976).
9. T. J. McCarthy, S.-P. Ngeyi, J.-H. Liao, D. C. DeGroot, T. Hogan, C. R. Kannewurf, and M. G. Kanatzidis, *Chem. Mater.* **5,** 331–340 (1993).
10. D. Schmitz and W. Bronger, *Z. Naturforsch. B Anorg. Chem. Org. Chem.* **29,** 438–439 (1974).
11. O. Glemser and M. Filcek, *Z. Anorg. Allg. Chem.* **279,** 321–323 (1955).
12. M. G. Kanatzidis, T. J. McCarthy, T. A. Tanzer, L.-H. Chen, L. Iordanidis, T. Hogan, C. R. Kannewurf, C. Uher, and B. Chen, *Chem. Mater.* **8,** 1465–1474 (1996).
13. D.-Y. Chung, K.-S. Choi, L. Iordanidis, J. L. Schindler, P. W. Brazis, C. R. Kannewurf, B. Chen, S. Hu, C. Uher, and M. G. Kanatzidis, *Chem. Mater.* **9,** 3060–3071 (1997).
14. Y. C. Wang and F. J. DiSalvo, *Chem. Mater.* **12,** 1011–1017 (2000).
15. D.-Y. Chung, T. Hogan, P. Brazis, M. Rocci-Lane, C. Kannewurf, M. Bastea, C. Uher, and M. G. Kanatzidis, *Science* **287,** 1024–1027 (2000).
16. M. Ohmasa and W. Nowacki, *Z. Kristallogr.* **137,** 422–432 (1973).
17. V. Kocman and E. W. Nuffield, *Acta Crystallogr. Sect. B Struct. Crystallogr. Cryst. Chem.* **29,** 2528–2535 (1973).
18. J. C. Portheine and W. Nowacki, *Z. Kristallogr.* **141,** 387–402 (1975).
19. R. D. Shannon, *Acta Crystallogr. Sect. A Cryst. Phys. Diffr. Theor. Gen. Crystallogr.* **32,** 751–767 (1976).
20. L. Iordanidis, J. L. Schindler, C. R. Kannewurf, and M. G. Kanatzidis, *J. Solid State Chem.* **143,** 151–162 (1999).
21. A. C. Sutorik, J. Albritton-Thomas, C. R. Kannewurf, and M. G. Kanatzidis, *J. Am. Chem. Soc.* **116,** 7706–7713 (1994).
22. A. C. Sutorik, J. Albritton-Thomas, T. Hogan, C. R. Kannewurf, and M. G. Kanatzidis, *Chem. Mater.* **8,** 751–761 (1996).
23. R. Patschke, P. Brazis, C. R. Kannewurf, and M. Kanatzidis, *Inorg. Chem.* **37,** 6562–6563 (1998).
24. P. Stoll, P. Dürichen, C. Näther, and W. Bensch, *Z. Anorg. Allg. Chem.* **624,** 1807–1810 (1998).
25. R. Patschke, P. Brazis, C. R. Kannewurf, and M. Kanatzidis, *J. Mater. Chem.* **8,** 2587–2589 (1998).
26. Bruker Analytical X-Ray Instruments, Inc., SMART Version 5.054 Data Collection and SAINT-Plus Version 6.02A Data Processing Software for the SMART System, Madison, WI, 2000.
27. G. M. Sheldrick, SHELXTL DOS/Windows/NT Version 5.10, Bruker Analytical X-Ray Instruments, Inc., Madison, WI, 2000.
28. Y. Le Page, *J. Appl. Crystallogr.* **20,** 264–269 (1987).
29. J. W. Lyding, H. O. Marcy, T. J. Marks, and C. R. Kannewurf, *IEEE Trans. Instrum. Meas.* **37,** 76–80 (1988).
30. H. O. Marcy, T. J. Marks, and C. R. Kannewurf, *IEEE Trans. Instrum. Meas.* **39,** 756–760 (1990).
31. A. E. Christuk, P. Wu, and J. A. Ibers, *J. Solid State Chem.* **110,** 330–336 (1994).
32. N. N. Greenwood and A. Earnshaw, "Chemistry of the Elements," Pergamon, New York, 1989.
33. P. Dürichen and W. Bensch, *Acta Crystallogr. Sect. C Cryst. Struct. Commun.* **54,** 706–708 (1998).